1-1-2020

Texture evolution induced by twinning and dynamic recrystallization in dilute Mg-1Sn-1Zn-1Al alloy during hot compression

Meijuan Hao
Taiyuan University of Technology

Weili Cheng
Taiyuan University of Technology

Lifei Wang
Taiyuan University of Technology

Ehsan Mostaed
Michigan Technological University, emostaed@mtu.edu

Liping Bian
Taiyuan University of Technology

See next page for additional authors

Follow this and additional works at: https://digitalcommons.mtu.edu/michigantech-p

Part of the Materials Science and Engineering Commons

Recommended Citation

Follow this and additional works at: https://digitalcommons.mtu.edu/michigantech-p

Part of the Materials Science and Engineering Commons

Authors

Meijuan Hao, Weili Cheng, Lifei Wang, Ehsan Mostaed, Liping Bian, Hongxia Wang, and Xiaofeng Niu

Full Length Article

Texture evolution induced by twinning and dynamic recrystallization in dilute Mg-1Sn-1Zn-1Al alloy during hot compression

Meijuan Hao[a], Weili Cheng[a,b,*], Lifei Wang[a,b], Ehsan Mostaed[c], Liping Bian[a,b], Hongxia Wang[a,b], Xiaofeng Niu[a,b]

[a] School of Materials Science and Engineering, Taiyuan University of Technology, Taiyuan 030024, China
[b] Shanxi Key Laboratory of Advanced Magnesium-Based Materials, Taiyuan University of Technology, Taiyuan 030024, China
[c] Department of Materials Science and Engineering, Michigan Technological University, Houghton, MI 49931, USA

Abstract

Texture evolution of an extruded dilute Mg-1Sn-1Zn-1Al alloy was thoroughly investigated based on the twinning and dynamic recrystallization (DRX) behavior via hot compression at a strain rate of 10 s^{-1} and temperature of 225°C. It was found that the types and intensities of the texture are strongly dependent on the fraction of twins and DRX modes as well as regions where sub-grain boundaries (sub-GBs) are intensively accumulated. At the initial stage of deformation, the formation of compression direction (CD)-tilted basal texture was mainly determined by the occurrence of $\{10\bar{1}2\}$ extension twins. As the strain increases, the variation in the texture intensity was greatly dominated by the DRX modes but the type of main texture remained unchanged. These findings are of great importance for texture modification of wrought Mg-Sn-based alloys during post-deformation.

1. Introduction

Due to the increasing demand for energy conservation and emission reduction, Mg alloys have attracted considerable attention in the automobile industry because of their low density and high specific strength [1,2]. However, their formability is limited primarily because only 2 independent slip systems on the basal slip plane can be activated for hexagonal close packed (HCP) crystal structure of Mg [3,4]. This fails to satisfy the Von-Mises criterion in which at least 5 independent slip systems are essential in the case of homogeneous deformation of metallic materials [5]. Indeed, strong basal texture arisen from insufficient active slip systems readily develops during hot deformation and thereby, causes tension/compression yield asymmetry in Mg-based alloys [6].

Therefore, the texture control is of paramount importance by which the performance of wrought Mg alloys could be tailored.

As one of the most important deformation mechanisms of hexagonal metals, twinning plays a momentous role in texture evolution. Firstly, twinning takes place at the initial stage of deformation to accommodate deformation along c-axis, and results in reorientation of parent grains [7,8]. Xu et al. [9] reported that $\{10\bar{1}2\}$ extension twins contribute to the randomization of basal texture during extrusion due to the reorientation of most parent grains by ∼86.3°. Moreover, profuse twin boundaries formed during the deformation can subdivide the original coarse grains via strong intersection of twins [10,11]. These fragmented fine grains can act as obstacles to dislocation glide, influencing on grain rotation during the further deformation.

In addition to the twinning, DRX has a significant impact on the texture evolution [12]. Three common DRX modes, in-

cluding twin-induced DRX (TDRX) [13], discontinuous DRX (DDRX) [14] and continuous DRX (CDRX) [15], occur in wrought Mg alloys. It was reported that CDRX grains can attenuate the extrusion-induced basal fiber texture [16]. On the other hand, DDRX grains show pronounced rotated orientations from the pre-existing grains, producing a weak texture during hot deformations [17-19]. Moreover, TDRX grains show new orientations and thereby, result in texture randomization [20].

Mg-Sn-based alloys have recently attracted increasing interest owing to Sn atoms contributing to microstructure modification and mechanical properties improvement [21]. Wang et al. [22] proposed that the addition of low amount of Sn ($\leq$ 1 wt.%) in Mg alloys is expected to improve the ductility and stretch formality at room temperature. Zou et al. [23], Bae et al. [24], and Jiang et al. [25] separately investigated the effect of the Sn addition on DRX behavior of as-homogenized Mg-5Zn-1Mn, Mg-Al-Zn and AZ80 alloy during hot deformation, respectively. The aforementioned research works are mainly associated with the accumulated strain energy caused by the inhibition effect of Mg_2Sn precipitates on grain boundary (GB) migration and/or dislocation glide in coarse-grained structure. However, only few works have focused on DRX behavior of extruded dilute Mg-Sn-based alloys with fine-grained structure, which could provide higher storage energy than their coarse-grained counterparts, ignoring the influence of particles [26,27]. Furthermore, the concurrent contributions of twinning and DRX to the texture evolution are still unclear for dilute Mg-Sn-based alloys during the hot deformation.

In the present work, we studied the simultaneous effects of twinning and DRX on the texture development in an extruded dilute Mg-1Sn-1Zn-1Al alloy during hot compression. It was reported that the critical resolved shear stress (CRSS) of twinning decreases sharply with increasing strain rates [28]. In addition, much effort is being put into the high-speed deformation with the aim of lowering the processing cost [19], and thus a relatively high strain rate of 10 s^{-1} was adopted in this study. The primary purpose of the present study is to clarify the following issues: (1) which type of twins will play a leading role during the hot compression? (2) which kind of DRX mechanisms will dominate the deformation process? (3) how do the twinning and DRX influence the formation of texture during compression? These findings are supposed to provide new insights into texture modification of Mg-Sn-based alloys during the hot deformation and therefore, better determine the processing parameters for post-deformation of dilute Mg-Sn-based alloys.

2. Experimental procedures

The alloy ingot with a nominal composition of Mg-1Sn-1Zn-1Al (wt.%) (TZA111) was prepared using commercially pure Mg, Sn, Zn, and Al (99.9 wt.%). The materials were melted in an electrical resistance furnace under a (SF$_6$ + CO$_2$) fluxing protection to avoid oxidation. The as-cast ingot with a diameter and length of 75 mm and 65 mm, respectively, was homogenized at 500°C for 3 h followed by water quenching.

Table 1
The conditions investigated for the hot compressed TZA111 alloy at different strains.

Sample Code	Sample condition
HC0.1	Hot compressed at a true strain of 0.1
HC0.3	Hot compressed at a true strain of 0.3
HC0.5	Hot compressed at a true strain of 0.5
HC0.7	Hot compressed at a true strain of 0.7

After preheating at 350°C for 45 min, the alloy ingot was extruded at 350°C with a ram speed of 0.1 mm/s and an extrusion ratio of 25.

Cylindrical compression specimens with a diameter of 8 mm and length of 12 mm were machined from the extruded rod with compression axis aligned with extrusion direction (ED). Compression tests were conducted using a Gleeble 3500-E machine at a temperature of 225°C and a strain rate of 10 s^{-1} with true strains ranging from 0.1 to 0.7. Table 1 summarizes the conditions investigated for the TZA111 alloy compressed at different strains. Once the compression tests were finished, the specimens were quenched in water to retain microstructural features during the hot compression.

All the compressed specimens were sectioned parallel to the CD for microstructural examinations. Optical microscopic (OM) observations of the samples were conducted using a Leica 2700 M optical microscope after a conventional metallographic procedure (including grinding, polishing, and etching in a solution of 1.5 g picric acid, 5 ml acetic acid, 5 ml H$_2$O, and 25 ml ethanol). Grain size and DRX fraction of the as-extruded sample were determined by Image-Pro Plus 6.0 software using 5 OM micrographs. The macroscopic texture of the as-extruded sample was measured using an X-ray diffractometer (XRD; Rigaku D/max-2500 PC) to obtain (0002) pole figure. Detailed microstructural characterizations were observed using transmission electron microscopy (TEM; JEM-2100F operated at 200 kV) and electron backscatter diffraction (EBSD; JEOL JSM-7000F operated at 20 kV). Micro-texture, fractions of DRX and twins, and grain size of as-compressed samples were statistically analyzed using HKL channel 5 software.

3. Results and Discussion

3.1. Initial microstructure and texture

Fig. 1 shows the optical micrograph along with (0002) pole figure of the extruded TZA111 alloy. The alloy exhibits a bimodal grain structure comprising of fine and equiaxed DRX grains with an average size and area fraction of 12.49 μm and 72.8%, respectively, along with coarse unDRX grains elongated along the ED (Fig. 1a). Furthermore, several secondary phase particles in the grain interior and/or along the GBs can be seen. In our previous study [29], these particles were detected as Sn containing phase originating from undissolved particles after homogenization treatment. Such particles may
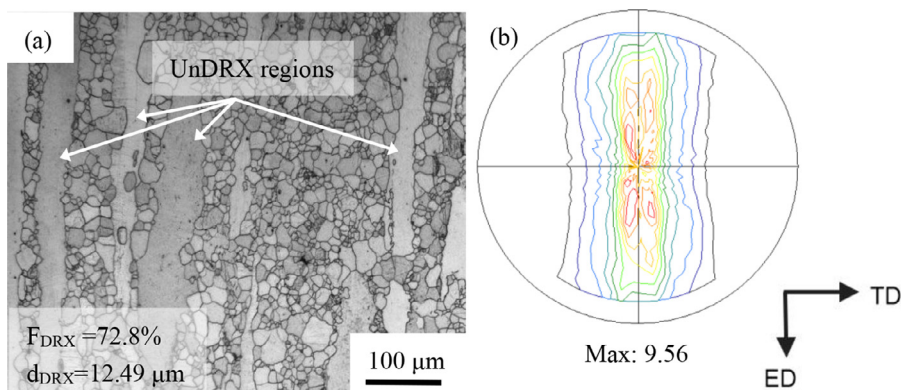
Fig. 1. (a) Optical microstructure, and (b) (0002) pole figure acquired by XRD of the extruded dilute TZA111 alloy with respect to the extrusion direction (ED) and transverse direction (TD). F_{DRX} and d_{DRX} denote area fraction and average size of DRX grains, respectively.
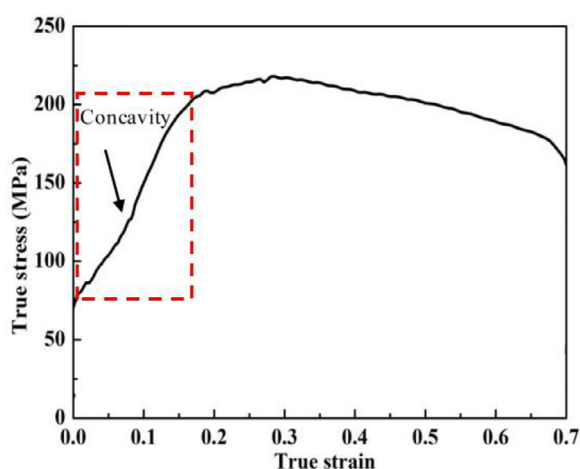

Fig. 2. True stress-strain curve of the extruded TZA111 alloy compressed at 225°C with a strain rate of 10 s^{-1}.

damage the mechanical properties, but they should exert an insignificant effect on the deformation mechanism due to their trace content. As seen in Fig. 1b, the extruded alloy features a typical extrusion texture where basal planes are parallel to the ED. In this case, $\{10\bar{1}2\}$ twinning will be activated in most of the grains when the compressive load is applied along the ED, as a compression produced perpendicular to the c-axis direction [30].

3.2. Flow behavior during compression

Fig. 2 shows the true stress-strain curve of the extruded TZA111 alloy samples compressed at 225°C with a strain rate of 10 s^{-1}. At the early stage of the deformation (highlighted by a red dashed rectangle), the flow curve exhibits a concave curvature, which is a characteristic of the $\{10\bar{1}2\}$ extension twinning-dominated deformation [31,32]. Then, the flow stress increases to a peak (218 MPa) followed by a decrease to lower stresses with increasing the strain. The increase of flow stress shows an intensive strain hardening behavior related to the impeding effect of twin boundaries on dislocation movements [33]. The decrease of flow stress may be ascribed

to dislocation annihilation caused by DRX and/or dynamic recovery [34].

3.3. Microstructure evolution during compression

3.3.1. Twinning behavior

Fig. 3 shows the inverse pole figure (IPF) maps and corresponding boundary misorientation maps of the investigated samples. Low angle GBs (LAGBs, 2~15°), high angle GBs (HAGBs, >15°), and twin boundaries, including $\{10\bar{1}2\}$ extension, $\{10\bar{1}1\}$ contraction and $\{10\bar{1}1\}$-$\{10\bar{1}2\}$ double twin boundaries, are marked in different colors (Fig. 3a-h). The angular deviation to determine the twin boundaries was within 5° of the ideal values. In addition, the volume fractions of different twin types for the compressed samples are listed in Table S1 in supplementary file.

For HC0.1 sample, almost all twins are detected as $\{10\bar{1}2\}$ extension twins (Fig. 3a-b), with the volume fraction being 16.7% (Table S1). The occurrence of extension twins is consistent with the concavity in the true stress-strain curve in Fig. 2. In the HC0.3 sample, the volume fraction of $\{10\bar{1}2\}$ extension twins considerably decreases alongside the activation of limited number of $\{10\bar{1}1\}$ contraction and $\{10\bar{1}1\}$-$\{10\bar{1}2\}$ double twins (total volume fraction: 1.89% as shown in Table S1) (Fig. 3c-d). Detailed boundaries misorientation angle distributions are presented in Fig. 4. As presented in Fig. 4a, the pronounced peaks in the range 85-90° about $<\bar{1}2\bar{1}0>$ axis and 55-60° about $<01\bar{1}0>$ axis suggest the occurrence of $\{10\bar{1}2\}$ extension twins and different $\{10\bar{1}2\}$ twin variants, verifying the intersection and coalescence of extension twins [30]. Distinguished peaks in the range 35-40° and 85-90° about $<\bar{1}2\bar{1}0>$ axis are attributed to the activation of $\{10\bar{1}1\}$-$\{10\bar{1}2\}$ double and $\{10\bar{1}2\}$ extension twins, respectively, in HC0.3 sample (Fig. 4b) [19]. It should be noted that HC0.5 and HC0.7 samples show no dominant misorientation in the range 35-40°, 55-60° and 85-90°, implying the presence of limited number of twins (Fig. 4c-d), which is in well agreement with boundary misorientation maps shown in Fig. 3e-h. It is therefore concluded that the extension twins are preferentially activated at the initial strain stage during the hot compression.
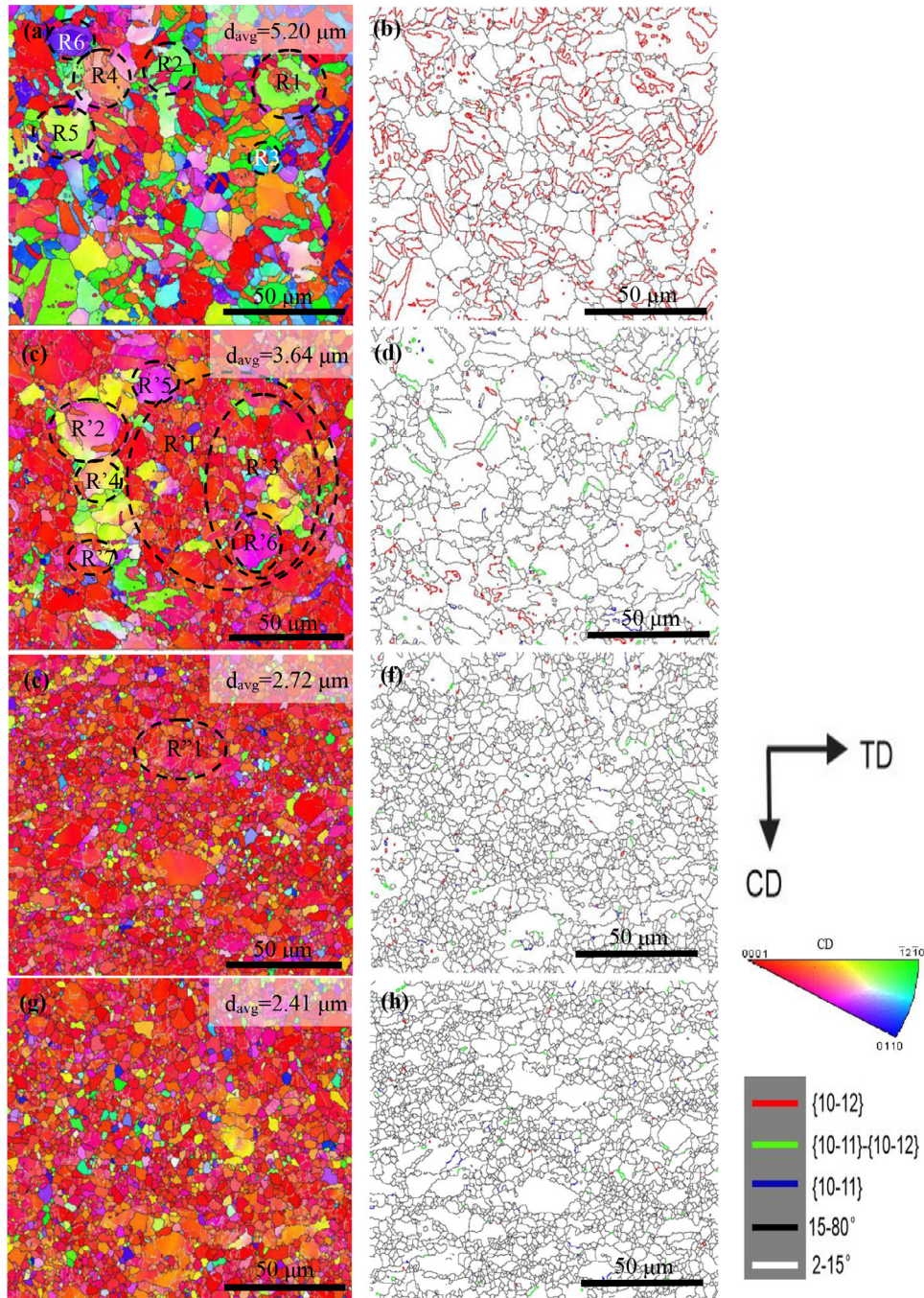
Fig. 3. The inverse pole figure (IPF) maps and corresponding boundary misorientation maps of: (a, b) HC0.1; (c, d) HC0.3; (e, f) HC0.5; and (g, h) HC0.7 samples. d_{avg} denotes the average grain size.

In order to have a better understanding about the twinning behavior of HC0.1 sample, certain typical regions (R1-R3) were selected from Fig. 3a, and enlarged as presented in Fig. 5a-c. As seen in Fig. 5a, the $\{10\bar{1}2\}$ twins lack the representative lenticular morphology due to their intersection/coalescence during the compression. Besides, ultrafine DRX grains with misorientations similar to that of $\{10\bar{1}2\}$ twins are found to occur in areas where huge number of sub-GBs are accumulated (as indicated by black lines in Fig. 5a). It can be inferred that this DRX behavior is related

to CDRX mechanism characterized by the successive absorption of dislocations into sub-GBs, leading to the formation of DRX grains separated with HAGBs [35,36]. It was previously reported that $\{10\bar{1}2\}$ twins promote the CDRX process indirectly owing to their GBs being quite mobile [37-39]. Hence, it is assumed that the extension twins are consumed by CDRX grains at higher strains. Jiang et al. [19] reported a similar phenomenon that the intersection and coalescence of $\{10\bar{1}2\}$ twins could trigger the formation of refined DRX grains. In R2 zone (Fig. 5b) it can be observed that two par-
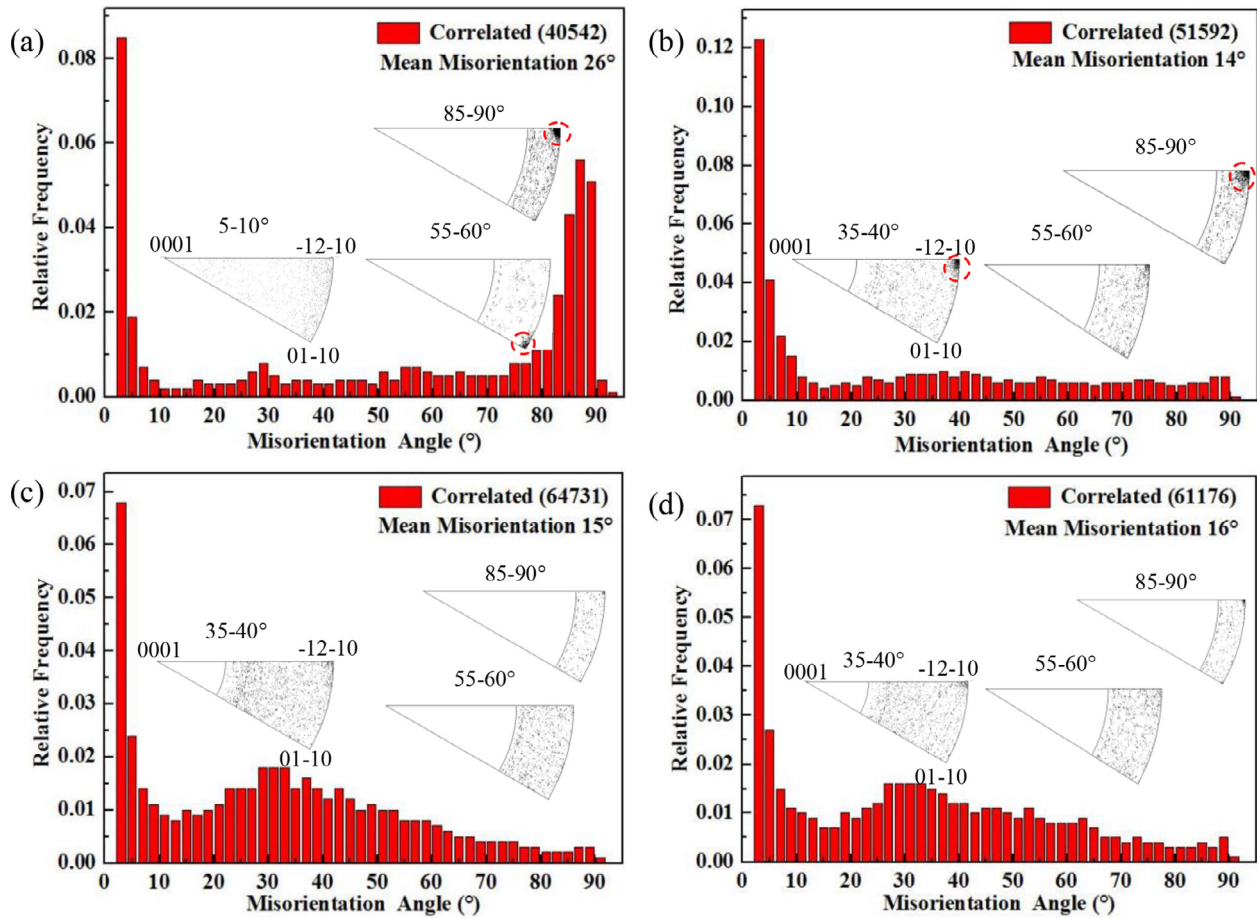
Fig. 4. Misorientation angle distributions of: (a) HC0.1; (b) HC0.3; (c) HC0.5; and (d) HC0.7 samples.
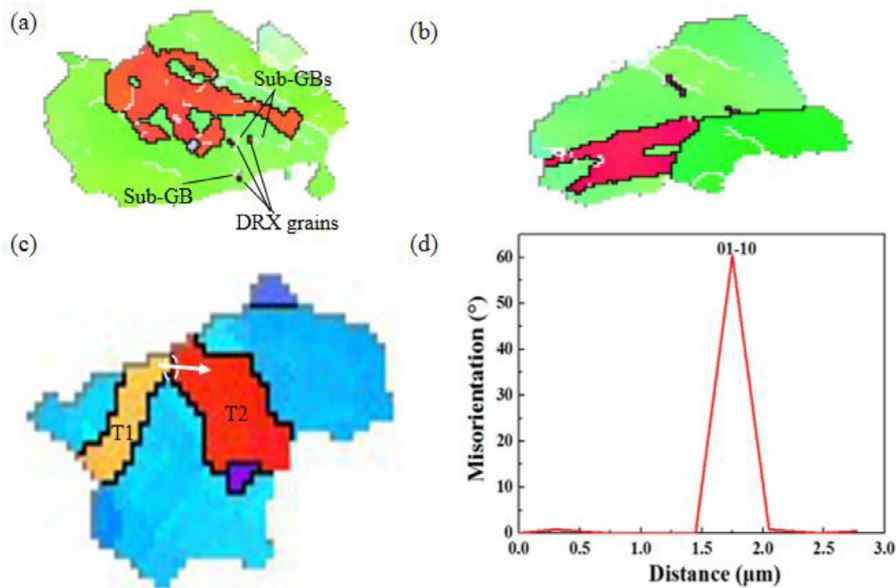

Fig. 5. The enlarged IPF maps selected from different regions in Fig. 3a: (a) R1; (b) R2; and (c) R3, indicating the extension twinning behavior in HC0.1 sample. (d) point-to-point misorientation angles along the direction indicated by white arrow in (c).
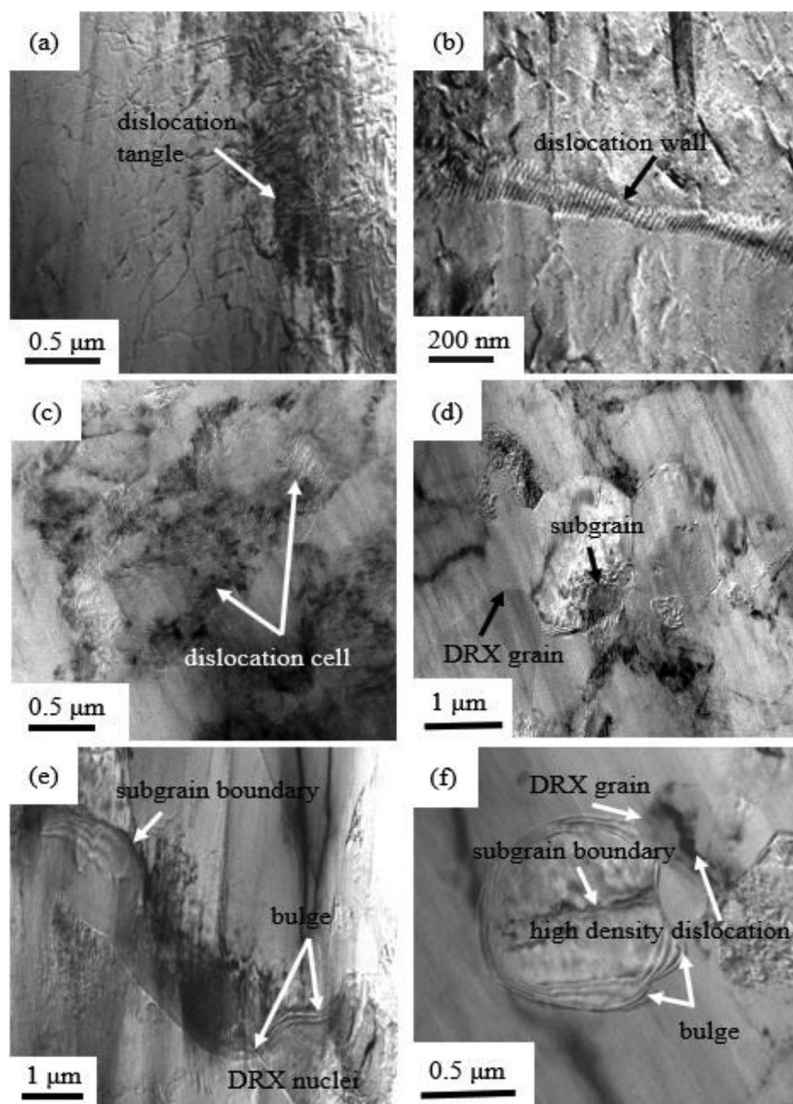
Fig. 6. TEM images of (a-d) HC0.3, and (e-f) HC0.5 samples showing: (a) dislocation tangle; (b) dislocation wall; (c) dislocation cell; (d) subgrain and DRX grain; (e) bulging grain boundary; and (f) sub-GBs subdividing the original grain with bulging grain boundary.

allel extension twin lamellas coalesced together, which can contribute to the formation of fine DRX grains [19]. It is well known that reduction of the grain size restricts the formation of twins due to the large obstructive effect of GBs on the twinning shear [40]. In the present work, an increase of the strain from 0.1 to 0.7 is accompanied by decrease of the average grain size from 5.20 μm to 2.41 μm through DRX, which results in reduction of the twin fraction to a large extent. R3 region (Fig. 5c) consists of two intersected {10$\bar{1}$2} twins, marked as T1 and T2, forming a{10$\bar{1}$2} twin variant with a misorientation angle of ∼60° and the misorientation axis is <01$\bar{1}$0>, as shown in Fig. 5d, which could impede the growth of preactivated twins [41,42].

3.3.2. DRX behavior

The nucleation mechanisms of DRX during the hot compression could be better perceived by TEM analysis. Fig. 6 shows the TEM images of HC0.3 and HC0.5 sam-

ples, and TEM data about HC0.1 and HC0.7 is not shown here for the sake of brevity. As seen, at the initial strain stage, severe dislocation tangles occur at the original GBs (Fig. 6a). When dislocation accumulation reaches a certain extent, merging and rearrangement through slip, climb and cross-slip of dislocations reduce the internal storage energy of the alloy [43], resulting in the formation of dislocation walls and cells (Fig. 6b-c). At higher amount of strains, the dislocation cells develop into single subgrains with LAGBs and eventually as depicted in Fig. 6d DRX grains with HAGBs form via progressive subgrain rotation [44,45]. It is therefore deduced that CDRX mechanism takes place in TZA111 alloy during the hot compressive deformation.

In addition, bulging GBs are identified in HC0.5 sample (Fig. 6e-f). Meanwhile, DRX nuclei emerge in the vicinity of the bulging GB (Fig. 6e). Sub-GBs subdivide the original grains with bulging GB (Fig. 6f). The aforementioned characteristics are typical signs of DDRX mechanism in the studied
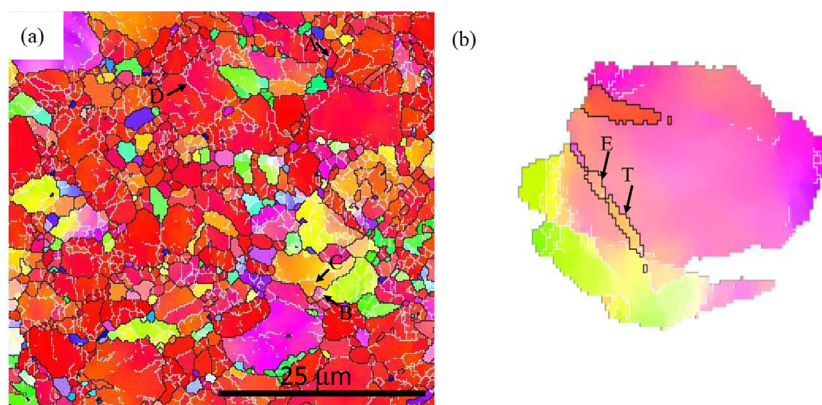
Fig. 7. Enlarged IPF maps selected from Fig. 3c showing evidence of different nucleation mechanisms of DRX: (a) R'1; and (b) R'2.

alloy [14]. Moreover, high dislocation density in DRX grains suggests that further GBs bulging may occur due to uneven stress distribution resulting from different dislocation density [43]. Similarly, Ponge et al. [46] revealed that further GBs bulging will be achieved for small DRX grains when new DRX grains scattered along all the pre-existing GBs.

EBSD observation results further show some features of DRX nucleation mechanisms in Fig. 7. GBs bulging and LAGBs that subdivide the bulged regime are the characteristics of DDRX (arrowed by A-C in Fig. 7a) [47]. Evidence of CDRX (a well-defined sub-grain structure expanded to the intragranular regions arrowed by D in Fig. 7a) is also presented. It should be noted that TDRX characterized by sub-GBs, which develop near the $\{10\bar{1}1\}$-$\{10\bar{1}2\}$ double twin (arrowed by T in Fig. 7b) and a TDRX grain (arrowed by E in Fig. 7b), is not abundant due to the limited fraction of the contraction and double twins. In other words, the contribution of TDRX to the texture evolution is negligible.

Although three DRX modes, including CDRX, DDRX, and TDRX are identified during the hot compression of TZA111 alloy, the dominant DRX mode during the deformation is still ambiguous. Indeed, firstly, CDRX plays a crucial role in strain accommodation during hot compression at intermediate temperatures of 200-250°C [48]. Secondly, the activation of extension twins is favorable for the subsequent CDRX procedure [19]. Finally, the mean misorientation decreases from 26° to 14° at the strains of 0.1 and 0.3, respectively, and eventually increases to 16° for HC0.7 sample (Fig. 4). This trend reflects the development of LAGBs into HAGBs. Accordingly, CDRX mode dominates the compression process for the extruded TZA111 alloy.

3.4. Effect of twinning and DRX on texture during compression

It is well documented that the DRX mechanism is one of the key determinants of texture evolution [12]. However, the impact of different DRX modes on the texture development is still controversial. For example, several studies have demonstrated that DDRX grains have orientations close to that of the original grains [49-51]. Nevertheless, Barnett et al. [18] proposed that DDRX grains would be deviated away from neighboring grains with misorientations of 5~20° in extruded Mg alloys. In the present study, it is indispensable to find out the effect of CDRX and/or DDRX on texture evolution during the hot compression.

Fig. 8 shows the effect of DDRX mechanism on the texture evolution in the selected region "R'3" in Fig. 3c. As indicated in Fig. 8a, sub-grains (S1-S3) forming along the bulged GBs will be subsequently transformed into new DDRX grains. These subgrains exhibit nearly similar orientations to that of parent grain "P2" in the (0002) pole figure (Fig. 8b). Interestingly, most of new DDRX grains form near the bulged GBs (G2, G3, and G6 in Fig. 8a) and at the triple junctions of the original grains (G1, G4, and G5 in Fig. 8a). Furthermore, as shown in Fig. 8b, DDRX grains (G1-G6) exhibit distinct texture orientation from their surrounding grains (P1-P6), resulting in the scattered distribution of CD-tilted basal texture.

In addition to DDRX, the effect of CDRX mechanism on the texture development needs to be addressed. Fig. 9a-b shows that the point-to-origin misorientations along the arrow AB are beyond 15°, implying that the misorientation accumulation and the progressive sub-grain rotation have been developed within the original grain, and thus the possibility of that the CDRX nucleation mechanism in this region [44]. Furthermore, new DRX grains are located in places where the sub-GBs are intensively accumulated. It can be therefore deduced that new DRX grains (G1'-G6') form through the CDRX nucleation mechanism (Fig. 9a). As indicated in Fig. 9c, CDRX grains (G1'-G6') are slightly reoriented from the parent grain "P" towards the CD, which contributes to the formation of CD-tilted basal texture in a certain degree.

Fig. 10 shows the (0002) pole figures of the total area, extension twin and DRX regions of the investigated samples, along with typical regions where large number of sub-GBs are accumulated (detailed information about the typical regions are exhibited in Fig. S1-S3), selected from Fig. 3a, c, e, and g, respectively. Considering the variation in volume fractions of twins and DRX during compression at different strains (Table S1), (0002) pole figures of the extension twins for HC0.1 sample, and DRX regions for HC0.3, HC0.5 and HC0.7 samples are displayed. In HC0.1 sample, due to the
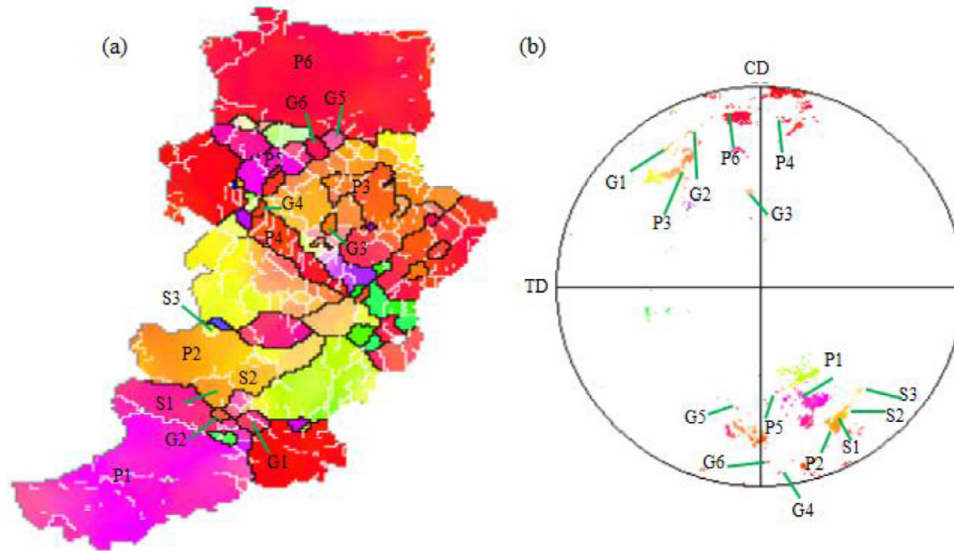
Fig. 8. Effect of DDRX mechanism on the texture evolution in the selected region R'3 in Fig. 3c: (a) IPF map; and (b) corresponding scattered (0002) pole figure.
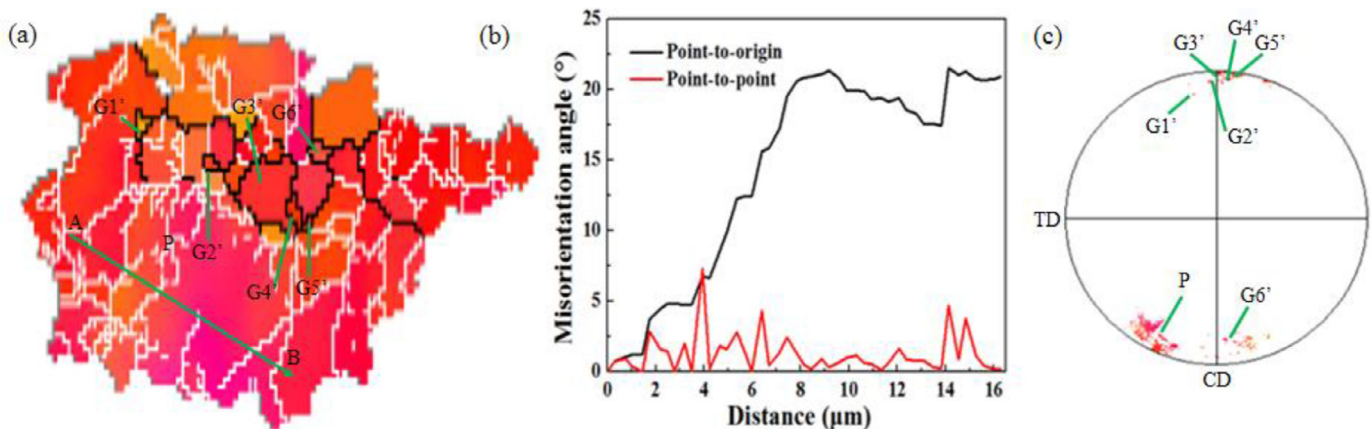

Fig. 9. Effect of CDRX mechanism on the texture evolution in the selected region R''1 in Fig. 3e: (a) IPF map; (b) line profiles of misorientation angles along the arrow AB in (a); and (c) the corresponding scattered (0002) pole figure.

activation of extension twins, a CD-tilted texture with one component tilting about 90° from the ND towards the CD is clear. In this sense, extension twins affect the texture evolution by reorienting the parent grains at the initial strain stage. In addition, some of the extension twins retain the initial extruded texture in which basal planes are parallel to the ED (indicated by a red dashed ellipse in the pole figure). It should be noted that few typical regions contribute to the formation of certain off-basal texture components in HC0.1 and HC0.3 samples. The peak intensity of CD-tilted basal texture (total area) increases from 11.08 to 16.05 multiples of random distribution (MRD) as the strain increases from 0.1 to 0.3. Firstly, the volume fraction of extension twins in HC0.3 sample decreased sharply compared to that in HC0.1 sample (16.7% vs. 2.07%). Therefore, it is easily deduced that texture randomization related to extension twinning could be weakened dramatically. Secondly, the occurrence of CDRX grains

in HC0.3 sample could strengthen CD-tilted basal texture to some extent (Fig. 9c). Finally, some typical regions, which contribute to the formation of certain scattered texture components, are consumed by DRX as the strain increases from 0.1 to 0.3. Namely, the increased texture intensity of total area is related to the reduced fraction of extension twins, higher fraction of CDRX and consumption of regions with off-basal texture components as the strain increases from 0.1 to 0.3. It can also be observed that asymmetrical double-peak texture was produced in HC0.3 sample due to the progress of DRX (DRX fraction: 8.55%), as reported by Jiang et al. [19].

At larger strains, the typical regions with the off-basal texture components are consumed by DRX and exhibit no off-basal orientations from the ND (HC0.5 and HC0.7 samples). This may be related to the fact that DRX occurs at sufficiently high strains (DRX fraction of 27.5% and 33.20% for HC0.5 and HC0.7, respectively.) and the typical regions are full of
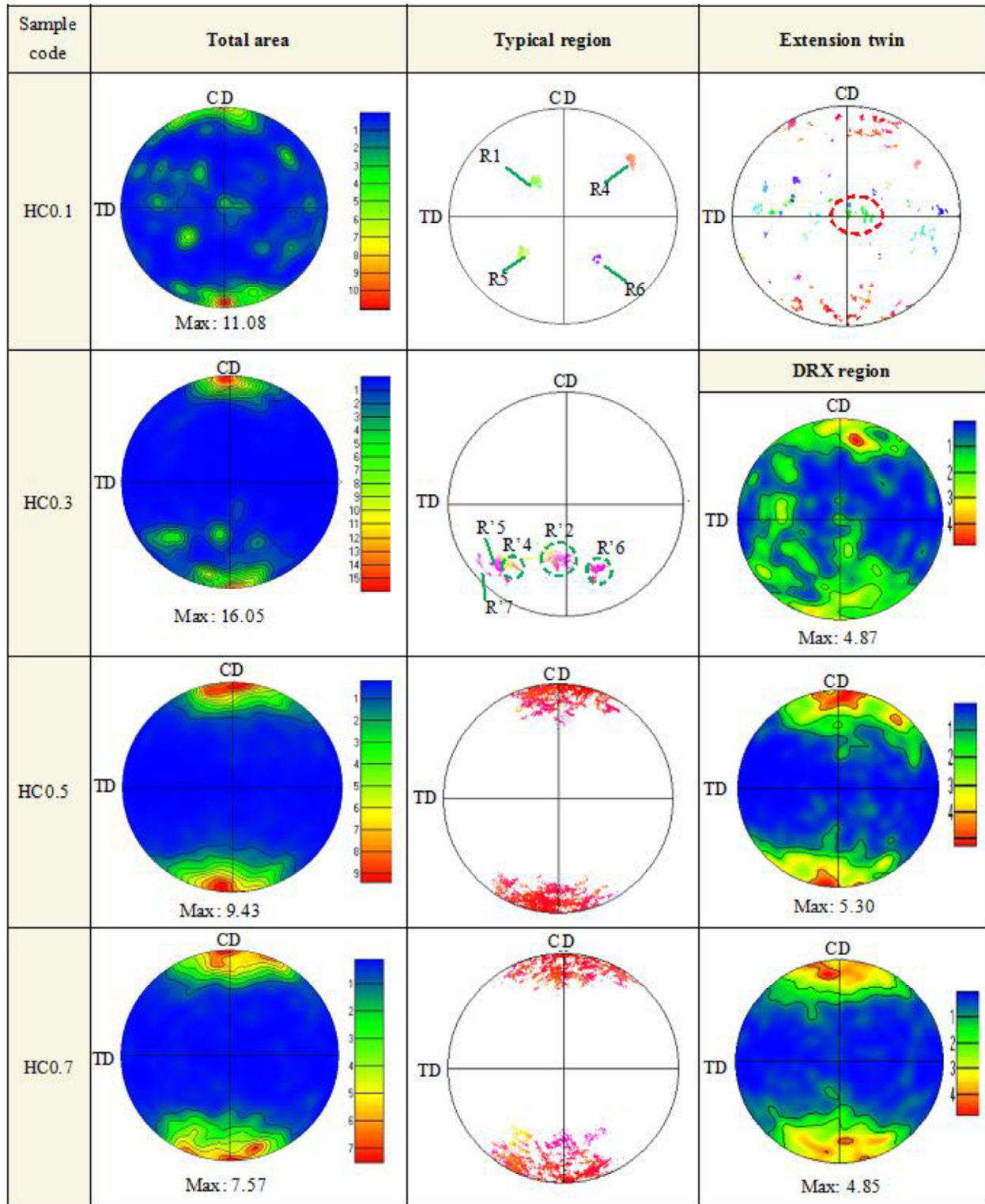
Fig. 10. (0002) pole figures of different regions, namely, overall, typical, extension twin and DRX areas of the hot compressed samples. Typical regions refer to those areas where sub-GBs are accumulated, selected from Fig. 3a, c, e, and g, respectively.

relatively large DRX grains showing a texture featuring basal planes perpendicular to the CD. In addition, as the strain increases from 0.3 to 0.7, the maximum CD-tilted basal texture intensity of DRX regions initially increases from 4.87 to 5.30 and then decreases to 4.85, implying that the CDRX mechanism has a significant contribution to the texture development in HC0.5. Indeed, as shown in Fig. 9, CDRX strengthens the CD-tilted texture, whilst the DDRX mechanism plays a cru-

cial role in the scattered distribution of CD-tilted basal texture of HC0.7 sample (Fig. 8). The large basal intensity areas with broader distribution towards the TD in HC0.5 sample are as a consequence of rotation of c-axis, which is ascribed to the twinning-induced parent grains reorientation for further dislocation slip (see the average Schmid factor values in Table S1) [25]. Combined effects of DRX (including CDRX and DDRX) and dislocation gliding result in a reduced maximum texture intensity in HC0.5 sample (from 16.05 to 9.43 MRD). For HC0.7 sample, the basal planes of the DRX grains are oriented towards the CD with an angle distribution of $\pm30°$ to the TD. Meanwhile, the total region of the sample shows several peaks splitting from the CD towards the TD in (0002) pole figure, which may be because of the occurrence of DDRX at larger strains and thus, the weakest texture intensity of 7.57 MRD is obtained.

4. Conclusions

In this study, the texture evolution in an extruded dilute TZA111 alloy was studied based on the twinning and DRX behavior during the high strain rate compression test with strains ranging from 0.1 to 0.7 at 225°C. It is interestingly found that CDRX mode is favorable to the formation of CD-tilted basal texture, while the DDRX mechanism plays a key role in the scattered distribution of CD-tilted basal texture. Furthermore, TDRX mechanism related to contraction and/or double twins has a minor influence on the overall texture evolution. As the strain increases from 0.1 to 0.3, the peak intensity of CD-tilted basal texture increases from 11.08 MRD to 16.05 MRD, which is related to the reduced fraction of extension twins, higher fraction of CDRX and consumption of regions with off-basal texture components. However, with increasing the strain from 0.3 to 0.7 the peak intensity of CD-tilted basal texture drops from 16.05 MRD to 7.57 MRD, which might be arisen from the combined effects of DRX (including CDRX and DDRX) and/or the lattice rotation of DRX grains caused by dislocation gliding during the continuous deformation.

Acknowledgments

Supplementary materials

Supplementary material associated with this article can be found, in the online version, at doi:10.1016/j.jma.2019.10.002.

References

[1] R. Islam, M. Haghshenas, Statistical optimization of stress level in Mg-Li-Al alloys upon hot compression testing, J. Magn. Alloys 7 (2019) 203–217.

[2] A. Javaid, F. Czerwinski, Effect of hot rolling on microstructure and properties of the ZEK100 alloy, J. Magn. Alloys 7 (2019) 27–37.

[3] M. Yuasa, N. Miyazawa, M. Hayashi, M. Mabuchi, Y. Chino, Effects of group II elements on the cold stretch formability of Mg–Zn alloys, Acta Mater. 83 (2015) 294–303.

[4] W.H. Liu, X. Liu, C.P. Tang, W. Yao, Y. Xiao, X.H. Liu, Microstructure and texture evolution in LZ91 magnesium alloy during cold rolling, J. Magn. Alloys 6 (2018) 77–82.

[5] T. Jin, Z. Zhou, J. Qiu, Z. Wang, D. Zhao, X. Shu, S. Yan, Investigation on the yield behavior of AZ91 magnesium alloy, J. Alloy. Comp. 738 (2018) 79–88.

[6] W. Jiang, J. Wang, W. Zhao, Q. Liu, D. Jiang, S. Guo, Effect of Sn addition on the mechanical properties and bio-corrosion behavior of cytocompatible Mg–4Zn based alloys, J. Magn. Alloys 7 (2019) 15–26.

[7] B. Song, R. Xin, N. Guo, Z. Chen, X. Yang, Q. Liu, Influence of basal slip activity in twin lamellae on mechanical behavior of Mg alloys, Mater. Lett. 176 (2016) 147–150.

[8] Y. Xin, M. Wang, Z. Zeng, M. Nie, Q. Liu, Strengthening and toughening of magnesium alloy by {10−12} extension twins, Scr. Mater. 66 (2012) 25–28.

[9] S.W. Xu, K. Oh-ishi, S. Kamado, T. Homma, Twins, recrystallization and texture evolution of a Mg–5.99Zn–1.76Ca–0.35Mn (wt.%) alloy during indirect extrusion process, Scr. Mater. 65 (10) (2011) 875–878.

[10] S.G. Hong, S.H. Park, C.S. Lee, Role of {10–12} twinning characteristics in the deformation behavior of a polycrystalline magnesium alloy, Acta Mater. 58 (2010) 5873–5885.

[11] H. Chen, T. Liu, D. Hou, D. Shi, Improving the mechanical properties of a hot-extruded AZ31 alloy by{10-12}twinning lamella, J. Alloy. Comp. 680 (2016) 191–197.

[12] J.P. Hadorn, R.P. Mulay, K. Hantzsche, S. Yi, J. Bohlen, D. Letzig, S.R. Agnew, Texture Weakening Effects in Ce-Containing Mg Alloys, Metall. Mater. Trans. A 44 (2012) 1566–1576.

[13] Y. Tian, H. Huang, G. Yuan, W. Ding, Microstructure evolution and mechanical properties of quasicrystal-reinforced Mg–Zn–Gd alloy processed by cyclic extrusion and compression, J. Alloy. Comp. 626 (2015) 42–48.

[14] Z. Shahri, A. Zarei-Hanzaki, H.R. Abedi, S.M. Fatemi-Varzaneh, An investigation to the hot deformation characteristics of AZ31 alloy through continuous cooling compression testing method, Mater. Des. 36 (2012) 470–476.

[15] B.J. Lv, J. Peng, Y.J. Wang, X.Q. An, L.P. Zhong, A.T. Tang, F.S. Pan, Dynamic recrystallization behavior and hot workability of Mg–2.0Zn–0.3Zr–0.9Y alloy by using hot compression test, Mater. Des. 53 (2014) 357–365.

[16] J.P. Hadorn, T.T. Sasaki, T. Nakata, T. Ohkubo, S. Kamado, K. Hono, Solute clustering and grain boundary segregation in extruded dilute Mg–Gd alloys, Scr. Mater. 93 (2014) 28–31.

[17] É. Martin, J.J. Jonas, Evolution of microstructure and microtexture during the hot deformation of Mg–3% Al, Acta Mater. 58 (2010) 4253–4266.

[18] M.R. Barnett, A. Sullivan, N. Stanford, N. Ross, A. Beer, Texture selection mechanisms in uniaxially extruded magnesium alloys, Scr. Mater. 63 (2010) 721–724.

[19] M.G. Jiang, H. Yan, R.S. Chen, Twinning, recrystallization and texture development during multi-directional impact forging in an AZ61 Mg alloy, J. Alloy. Comp. 650 (2015) 399–409.

[20] S. Yi, I. Schestakow, S. Zaefferer, Twinning-related microstructural evolution during hot rolling and subsequent annealing of pure magnesium, Mater. Sci. Eng. A 516 (2009) 58–64.

[21] B.-C. Suh, J.H. Kim, J.H. Bae, J.H. Hwang, M.-S. Shim, N.J. Kim, Effect of Sn addition on the microstructure and deformation behavior of Mg-3Al alloy, Acta Mater. 124 (2017) 268–279.

[22] Q. Wang, Y. Shen, B. Jiang, A. Tang, Y. Chai, J. Song, T. Yang, G. Huang, F. Pan, A good balance between ductility and stretch formability of dilute Mg-Sn-Y sheet at room temperature, Mater. Sci. Eng. A 736 (2018) 404–416.

[23] J. Zou, J. Chen, H. Yan, W. Xia, B. Su, Y. Lei, Q. Wu, Effects of Sn addition on dynamic recrystallization of Mg-5Zn-1Mn alloy during high strain rate deformation, Mater. Sci. Eng. A 735 (2018) 49–60.

[24] S.W. Bae, S.H. Kim, J.U. Lee, W.K. Jo, W.H. Hong, Improvement of mechanical properties and reduction of yield asymmetry of extruded Mg-Al-Zn alloy through Sn addition, J. Alloy. Comp. 766 (2018) 748–758.

[25] L.Y. Jiang, W.J. Huang, D.F. Zhang, F. Guo, H.S. Xue, J.Y. Xu, F.S. Pan, Effect of Sn on the microstructure evolution of AZ80 magnesium alloy during hot compression, J. Alloy. Comp. 727 (2017) 205–214.

[26] W. Cheng, Y. Bai, S. Ma, L. Wang, H. Wang, H. Yu, Hot deformation behavior and workability characteristic of a fine-grained Mg–8Sn–2Zn–2Al alloy with processing map, J. Mater. Sci. Technol. 35 (2019) 1198–1209.

[27] Y. Chai, B. Jiang, J. Song, B. Liu, G. Huang, D. Zhang, F. Pan, Effects of Zn and Ca addition on microstructure and mechanical properties of as-extruded Mg-1.0Sn alloy sheet, Mater. Sci. Eng. A 746 (2019) 82–93.

[28] J. Jeong, M. Alfreider, R. Konetschnik, D. Kiener, S.H. Oh, In-situ TEM observation of {10-12} twin-dominated deformation of Mg pillars: Twinning mechanism, size effects and rate dependency, Acta Mater. 158 (2018) 407–421.

[29] W. Cheng, Y. Zhang, S. Ma, S. Arthanari, Z. Cui, H.X. Wang, L. Wang, Tensile Properties and Corrosion Behavior of Extruded Low-Alloyed Mg-1Sn-1Al-1Zn Alloy: The Influence of Microstructural Characteristics, Mater 11 (2018) 1157.

[30] Y.R. Zhao, L.L. Chang, J. Guo, Y.P. Jin, Twinning behavior of hot extruded AZ31 hexagonal prisms during uniaxial compression, J. Magn. Alloys 7 (2019) 90–97.

[31] S.H. Park, S.G. Hong, J.H. Lee, Y.H. Huh, Texture evolution of rolled Mg–3Al–1Zn alloy undergoing a {10-12} twinning dominant strain path change, J. Alloy. Comp. 646 (2015) 573–579.

[32] S. Hyuk Park, S.-G. Hong, C.S. Lee, In-plane anisotropic deformation behavior of rolled Mg–3Al–1Zn alloy by initial {10–12} twins, Mater. Sci. Eng. A 570 (2013) 149–163.

[33] L. Jiang, J.J. Jonas, A.A. Luo, A.K. Sachdev, S. Godet, Influence of {10-12} extension twinning on the flow behavior of AZ31 Mg alloy, Mater. Sci. Eng. A 445-446 (2007) 302–309.

[34] M. Shalbafi, R. Roumina, R. Mahmudi, Hot deformation of the extruded Mg–10Li–1Zn alloy: Constitutive analysis and processing maps, J. Alloy. Comp. 696 (2017) 1269–1277.

[35] T. Al-Samman, K.D. Molodov, D.A. Molodov, G. Gottstein, S. Suwas, Softening and dynamic recrystallization in magnesium single crystals during c-axis compression, Acta Mater. 60 (2012) 537–545.

[36] M.T. Pérez-Prado, J.A. del Valle, J.M. Contreras, O.A. Ruano, Microstructural evolution during large strain hot rolling of an AM60 Mg alloy, Scr. Mater. 50 (2004) 661–665.

[37] M.G. Jiang, H. Yan, R.S. Chen, Microstructure, texture and mechanical properties in an as-cast AZ61 Mg alloy during multi-directional impact forging and subsequent heat treatment, Mater. Des. 87 (2015) 891–900.

[38] Z.R. Zeng, M.Z. Bian, S.W. Xu, C.H.J. Davies, N. Birbilis, J.F. Nie, Texture evolution during cold rolling of dilute Mg alloys, Scr. Mater. 108 (2015) 6–10.

[39] M.D. Nave, M.R. Barnett, Microstructures and textures of pure magnesium deformed in plane-strain compression, Scr. Mater. 51 (2004) 881–885.

[40] Y. Xin, X. Zhou, L. Lv, Q. Liu, The influence of a secondary twin on the detwinning deformation of a primary twin in Mg–3Al–1Zn alloy, Mater. Sci. Eng. A 606 (2014) 81–91.

[41] S.H. Park, S.-G. Hong, C.S. Lee, Activation mode dependent {10−12} twinning characteristics in a polycrystalline magnesium alloy, Scr. Mater. 62 (2010) 202–205.

[42] S.H. Park, J.H. Lee, B.G. Moon, B.S. You, Tension–compression yield asymmetry in as-cast magnesium alloy, J. Alloy. Comp. 617 (2014) 277–280.

[43] Y. Wu, M. Zhang, X. Xie, J. Dong, F. Lin, S. Zhao, Hot deformation characteristics and processing map analysis of a new designed nickel-based alloy for 700°C A-USC power plant, J. Alloy. Comp. 656 (2016) 119–131.

[44] Y.C. Lin, X.-Y. Wu, X.-M. Chen, J. Chen, D.-X. Wen, J.-L. Zhang, L.-T. Li, EBSD study of a hot deformed nickel-based superalloy, J. Alloy. Comp. 640 (2015) 101–113.

[45] W.L. Cheng, Q.W. Tian, H. Yu, B.S. You, H.X. Wang, Optimum parameters and kinetic analysis for hot working of a homogenized Mg–8Sn–1Al–1Zn alloy, Mater. Des. 85 (2015) 762–770.

[46] D. Ponge, G. Gottstein, Necklace formation during dynamic recrystallization: mechanisms and impact on flow behavior, Acta Mater. 46 (1998) 69–80.

[47] E. Dogan, M.W. Vaughan, S.J. Wang, I. Karaman, G. Proust, Role of starting texture and deformation modes on low-temperature shear formability and shear localization of Mg–3Al–1Zn alloy, Acta Mater. 89 (2015) 408–422.

[48] A. Galiyev, R. Kaibyshev, G.J. Gottstein, Correlation of plastic deformation and dynamic recrystallization in magnesium alloy ZK60, Acta Mater. 49 (2001) 1199–1207.

[49] J. Zhang, B. Chen, C. Liu, An investigation of dynamic recrystallization behavior of ZK60-Er magnesium alloy, Mater. Sci. Eng. A 612 (2014) 253–266.

[50] T. Al-Samman, G. Gottstein, Dynamic recrystallization during high temperature deformation of magnesium, Mater. Sci. Eng. A 490 (2008) 411–420.

[51] H. Borkar, R. Gauvin, M. Pekguleryuz, Effect of extrusion temperature on texture evolution and recrystallization in extruded Mg–1% Mn and Mg–1% Mn–1.6%Sr alloys, J. Alloy. Comp. 555 (2013) 219–224.